

Metathesis

Metathesis of 1-Butene to Propene over Mo/Al₂O₃@SBA-15: Influence of Alumina Introduction Methods on Catalytic PerformanceDazhou Zhang,^[a, b] Xiujie Li,^{*[a]} Shenglin Liu,^[a] Xiangxue Zhu,^[a] Fucun Chen,^[a] and Longya Xu^{*[a]}

Abstract: A series of Mo-based catalysts for 1-butene metathesis to propene were prepared by supporting Mo species on SBA-15 premodified with alumina. The effects of the method of introduction of the alumina guest to the host SBA-15 on the location of the Mo species and the corresponding metathesis activity were studied. As revealed by N₂ adsorption isotherms and TEM results, well-dispersed alumina was formed on the pore walls of SBA-15 if the ammonia/water vapor induced hydrolysis (NIH) method was employed. The Mo species preferentially interacted with alumi-

na instead of SBA-15, as evidenced by X-ray photoelectron spectroscopy, time-of-flight secondary-ion mass spectrometry, and IR spectroscopy of adsorbed pyridine. Furthermore, new Brønsted acid sites favorable for the dispersion of the Mo species and low-temperature metathesis activity were generated as a result of the effective synergy between the alumina and SBA-15. The Mo/Al₂O₃@SBA-15 catalyst prepared by the NIH method showed higher metathesis activity and stability under the conditions of 120 °C, 0.1 MPa, and 1.5 h⁻¹ than catalysts prepared by other methods.

Introduction

Recently, the interest in propene, as an important building block material in the petrochemical industry, has increased owing to the strongly growing demand for propene derivatives. Traditional ways to produce propene are mainly based on naphtha steam cracking and fluid catalytic cracking as a coproduct in the petrochemical industry, and these methods are currently not sufficient to meet the strong market demand around the world.^[1] Since the beginning of this century, the feedstock of steam cracking has been shifting to lighter ethane, especially in North America because of the emergence of shale gas as an unconventional fossil resource, and this will further reduce the productivity of propene.^[2] Consequently, several other processes, such as methanol to olefin,^[3] propane dehydrogenation,^[4] catalytic cracking of C₄⁺ olefins,^[5] and olefin metathesis reactions,^[1,6,7] have been revived and developed for the production of propene. Given that olefin meta-

thesis could easily regulate the stocks of light olefins on the market demand, its industrial application between ethene and 2-butene to propene was realized in the 1970s.^[8,9] It has been suggested that autometathesis of 1-butene, that is, isomerization of 1-butene into 2-butene followed by cross-metathesis of 1-butene and 2-butene, should be a more attractive and promising way to enhance the productivity of propene as a result of the abundance of butene as a feedstock in the petrochemical industry.^[10–15]

Usually, traditional porous alumina, silica, or their composites are applied as supports during the preparation of metathesis catalysts. For example, Wang et al.^[11] studied the autometathesis of 1-butene on a WO₃/SiO₂ catalyst under the reaction conditions of 350 °C, weight hourly space velocity (WHSV) = 0.36 h⁻¹, and 0.5 MPa, and an initial propene yield of 32.7% was obtained. Harmase et al.^[15] deposited W species on acidic alumina–silica composite supports, and a maximum propene yield of 31.6% was realized at 450 °C and 0.085 MPa. Recently, Mazoyer et al.^[13] developed a catalyst with tungsten hydride supported on alumina (WH₃/Al₂O₃) through a surface organometallic chemistry method. This method allowed better molecular design of the active site, and preferable propene productivity was obtained in the autometathesis of 1-butene. In addition, some easy and effective methods, for example, non-hydrolytic sol–gel^[7] and the one-pot aerosol route,^[12] have also been developed, and the catalysts exhibit high activities at low temperatures.

SBA-15 is a mesoporous silica with a large surface area and an ordered pore structure;^[16] it has drawn great attention since its discovery.^[17,18] For example, a W-substituted mesoporous

[a] D. Zhang, Dr. X. Li, Prof. S. Liu, Prof. X. Zhu, F. Chen, Prof. L. Xu
State Key Laboratory of Catalysis
Dalian Institute of Chemical Physics
Chinese Academy of Sciences
Dalian 116023 (P.R. China)
Fax: (+86) 411-84379279
E-mail: xiujieli@dicp.ac.cn
lyxu@dicp.ac.cn

[b] D. Zhang
University of Chinese Academy of Sciences
Beijing 100049 (P.R. China)

Supporting Information for this article is available on the WWW under <http://dx.doi.org/10.1002/asia.201500351>.

SBA-15 (W-SBA-15) metathesis catalyst has been synthesized, and it showed excellent catalytic performance in the autometathesis of 1-butene to propene.^[19–21] However, a reaction temperature higher than 350 °C was still needed. Balcar et al.^[22–24] prepared many W-, Mo-, and Re-based catalysts supported on mesoporous silica and studied their catalytic performance in olefin metathesis. However, only the pure SBA-15 component was used as a support in their earlier reports.

The development of a highly efficient heterogeneous metathesis catalyst has been attracting the interest of researchers.^[1,25–28] It is known that alumina is an interesting and important material owing to its tunable surface acidity/basicity and its mechanical strength, and it has been widely used in the petrochemical industry as a support and catalyst. However, to our knowledge, there are no related reports outlining the use of alumina-modified SBA-15 as a support for the autometathesis of 1-butene. In this study, guest alumina was introduced onto/into the SBA-15 host to combine the acidity of alumina with the advantageous mesoporous structure of SBA-15. Thus, a novel Mo-based metathesis catalyst was developed. In addition, the effects of the different introduction methods on the physicochemical properties of the alumina–SBA-15 composite support and the Mo-based catalysts are discussed in detail. Relations between Mo dispersion on the support and the catalytic performance in the autometathesis of 1-butene were elucidated.

Results and Discussion

Characterization of the supports

Figure 1a shows the N₂ adsorption/desorption isotherm results of the different composite supports. Pristine mesoporous SBA-15 exhibits a typical type IV N₂ isotherm with an H1-type hysteresis loop according to the IUPAC classification.^[29] The amount of adsorbed N₂ decreased after introducing alumina, but yet the amount was still higher than that of the pure γ -Al₂O₃ support. The type IV N₂ isotherm is observed for all the alumina-coated samples, which indicates that the mesoporous structure of SBA-15 was preserved after introducing alumina. Notably, the shape of the hysteresis loop was greatly altered depending on the coating method. To be specific, M-AS-30 obtained by mechanical grinding (MG) exhibited two-step capillary evaporation in the desorption branch of the hysteresis loop, probably as a result of the presence of two different types of pores.^[30] According to the pore-diameter distribution results (Figure 1b), the peak value of M-AS-30 was close to that of pristine SBA-15. Thus, we could tentatively speculate that most of the introduced alumina accumulated outside the mesopores of the SBA-15 host. The fact that small amounts of alumina species migrated into the mesopores cannot be excluded because of the calcination treatment at 500 °C. As to C-AS-30 and W-AS-30, the type of hysteresis loop changed from H1 to H2. Generally, the H2 hysteresis loop can be attributed to locally blocked or ink-bottle pores.^[31,32] By applying the same viewpoint to C-AS-30 and W-AS-30, variation of the isotherms may be associated with pore blockage by the alumina particles or

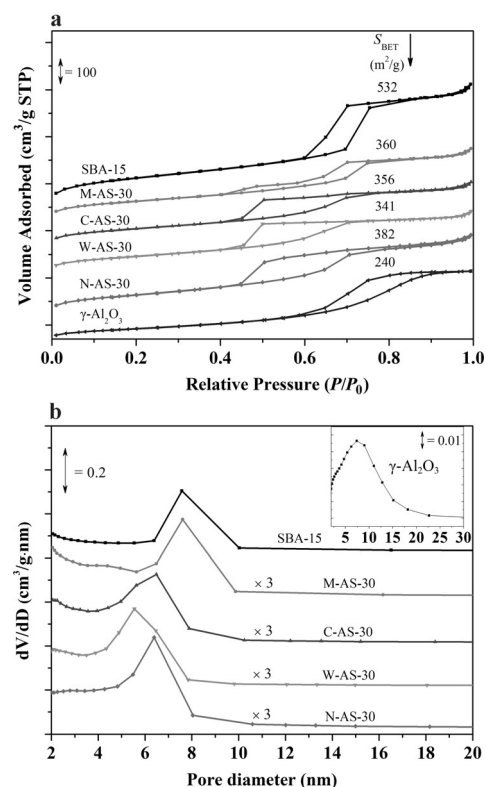


Figure 1. a) N₂ adsorption/desorption isotherms and b) pore-diameter distribution of the pristine SBA-15 and alumina premodified composite samples. (Plots are offset vertically for clarity.)

aggregates formed inside the mesopores. In addition, the degree of pore blocking was different between the two samples, as evidenced by their different pore-diameter distributions (Figure 1b). Interestingly, careful observation of the isotherm shape of the sample N-AS-30 indicated that the steepness of the desorption branch in the capillary condensation region improved. This change was also reflected by the narrower pore-diameter distribution, as shown in Figure 1b. These facts indicated that the introduced alumina was highly dispersed on the pore walls of SBA-15 through the ammonia/water vapor-induced hydrolysis (NIH) method, which is in good agreement with previous reports.^[30,33]

The low-angle XRD patterns of pristine SBA-15 and the four alumina-coated SBA-15 samples are shown in Figure 2a. The characteristic (100), (110), and (200) reflections corresponding to the hexagonal mesoporous structure can be clearly observed in the SBA-15, M-AS-30, and N-AS-30 samples, respectively, whereas the (110) and (200) reflections are barely visible in the C-AS-30 and W-AS-30 samples. This may be explained by the fact that pore blockage or improper coating on the pore walls of SBA-15 could result in a broader distribution of the electron density in the unit cell, which would lead to a decrease in the intensity at higher angle reflections;^[30] this implies that the mesopores may be blocked by the loaded alumina upon employing the conventional impregnation (CI) and water vapor-induced hydrolysis (WIH) methods. From the wide-angle XRD patterns (Figure 2b), no γ -Al₂O₃ phase was observed in the four samples.

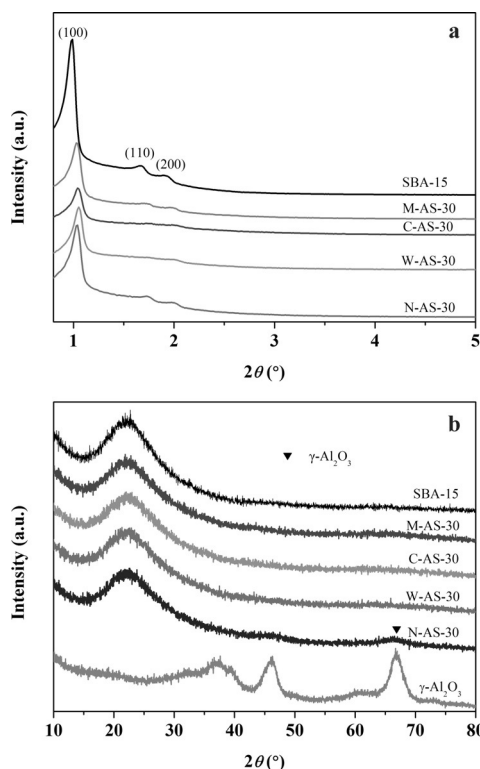


Figure 2. a) Low-angle and b) wide-angle XRD patterns of the pristine SBA-15 and alumina premodified composite samples.

TEM is an important and direct technique to characterize the mesopores of SBA-15. As shown in Figure 3a, some amorphous alumina aggregates are located outside the mesopores of M-AS-30 besides the highly ordered mesopore channel of SBA-15. This was not observed for N-AS-30 prepared by the NIH method, which indicated that alumina was highly dispersed on SBA-15. Prepared N-AS-30 can also be denoted as $\text{Al}_2\text{O}_3@\text{SBA-15}$, and consequently, most of the guest alumina is uniformly and highly dispersed on the SBA-15 host.

The states of the Al species in the composite materials were also investigated by ^{27}Al magic angle spinning (MAS) NMR spectroscopy. As shown in Figure 4, three distinct signals centered at $\delta = 61$, 33, and 5 ppm are observed for M-AS-30, C-AS-30, and W-AS-30, which can be assigned to tetrahedrally (Al_{Td}), pentahedrally (Al_{Pd}), and octahedrally (Al_{Oh}) coordinated Al species, respectively.^[34,35] The Al species in tetrahedral coordina-

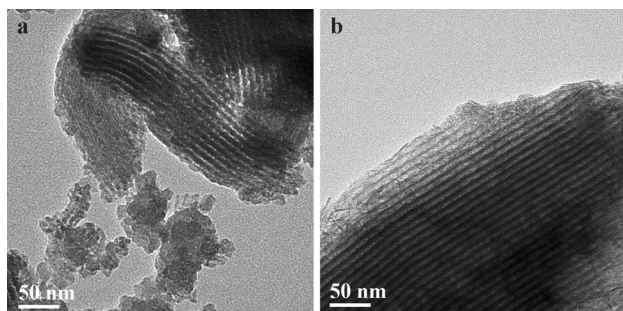


Figure 3. TEM images of a) M-AS-30 and b) N-AS-30.

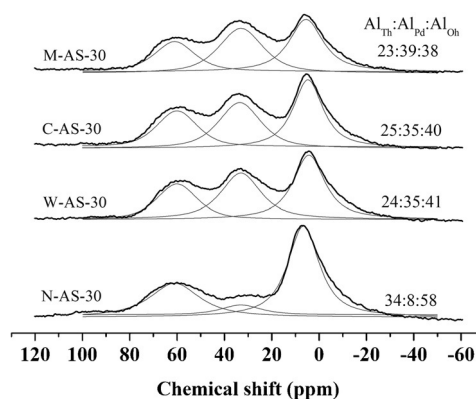


Figure 4. ^{27}Al MAS NMR spectra of the alumina premodified composite samples.

tion are approximately 23–25% from the deconvolution analysis. The presence of higher amounts of Al_{Pd} atoms indicates the local arrangement of the aluminum atoms is quite different from that in conventional $\gamma\text{-Al}_2\text{O}_3$, as the spectrum of the latter is mostly made up of Al_{Td} and Al_{Oh} contributions ($\approx 30:70$ ratio, as shown in Figure S1, Supporting Information).^[36] Hence, it may be concluded that larger amounts of the amorphous alumina-like phase was formed on the M-AS-30, C-AS-30, and W-AS-30 samples, which is usually suggested to be located at the interface between an aluminosilicate and an alumina phase.^[37–39] Interestingly, as to the N-AS-30 sample, the intensity of the Al_{Pd} contribution dramatically decreased to 8%, whereas the contribution of the Al_{Td} atoms increased to 34%.

It is known that the formation of Si–O–Al linkages is closely associated with resultant bridged hydroxy groups. Thus, the nature of the surface hydroxy groups was evaluated after thermal treatment at 350 °C. As shown in Figure 5, the diffuse reflectance infrared Fourier transform (DRIFT) spectrum of SBA-15 features a distinct band at $\tilde{\nu} = 3747\text{ cm}^{-1}$ resulting from the isolated Si–OH (silanol) groups. The intensity of this band decreases for the M-AS-30 sample, which is indicative of the consumption of the silanol groups during alumina coating by the

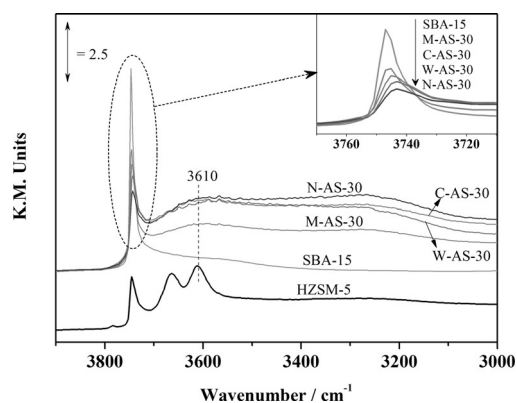


Figure 5. DRIFT spectra in the hydroxy region of the pristine SBA-15 and alumina premodified composite samples. The spectra were measured at 30 °C after pretreatment in Ar at 350 °C for 0.5 h. For comparison, the spectrum of HZSM-5 is also included.

MG method, as already reported in Ref. [40]. The intensity of this band decreased further for C-AS-30 and W-AS-30, and the lowest intensity was observed for N-AS-30. The decreasing trend of the band intensity is related to the consumption of silanol groups as a result of their interaction with alumina. It is well documented that bridging hydroxy groups in zeolites, closely associated with Brønsted acid sites, are observed in the range of $\tilde{\nu} = 3600$ to 3640 cm^{-1} (e.g., HZSM-5 zeolite, Figure 5). No such remarkable characteristic band could be detected, and there was only a broad absorption band between $\tilde{\nu} = 3700$ and 3500 cm^{-1} over all the alumina-coated samples. To further confirm the formation of Si–O–Al linkages, which is similar to the tetrahedral framework in the aluminosilicate zeolite, temperature-programmed desorption of ammonia (NH_3 -TPD) and infrared spectroscopy of adsorbed pyridine (Py-IR) experiments were performed to understand the acidic properties of the alumina-modified SBA-15 samples, especially the Brønsted acid sites.

The NH_3 -TPD results of pristine SBA-15 and the alumina-modified SBA-15 supports are shown in Table 1 and Figure S2. Clearly, the acid density on SBA-15 is low. The NH_3 -TPD curve of $\gamma\text{-Al}_2\text{O}_3$ features only one broad desorption peak at approximately $T = 260^\circ\text{C}$, and it can primarily be ascribed to ammonia adsorbed on coordinatively unsaturated electron-deficient aluminum cations generated by surface dehydroxylation/deoxygenation.^[41] As to all of the alumina-modified SBA-15 samples, the number of acid sites greatly increased relative to the number of acid sites on pristine SBA-15, and the shapes of the NH_3 -TPD profiles are similar to that of $\gamma\text{-Al}_2\text{O}_3$. According to quantitative analysis from the NH_3 -TPD experiment (Table 1), the total acid amount decreased in the following sequence: N-AS-30 > W-AS-30 > $\gamma\text{-Al}_2\text{O}_3$ > C-AS-30 > M-AS-30 > SBA-15. This sequence implies that the acidity of the supports is strongly dependent on the distribution of alumina, and new acid sites

may be generated after introducing alumina on SBA-15, especially over the N-AS-30 and W-AS-30 samples.

A Py-IR experiment was performed to distinguish the types of acid sites. As shown in Figure 6, different signals are observed in the spectra in the region of $\tilde{\nu} = 1700$ to 1400 cm^{-1} . Referring to Refs. [42,43], the bands at $\tilde{\nu} = 1445$ and 1595 cm^{-1} can be assigned to pyridine hydrogen bonded by surface hydroxy groups (e.g., Si–OH), the bands at $\tilde{\nu} = 1451$ and 1620 cm^{-1} can be assigned to pyridine adsorbed on strong Lewis acid sites, the band at $\tilde{\nu} = 1577 \text{ cm}^{-1}$ can be assigned to pyridine adsorbed on weak Lewis acid sites, and bands at $\tilde{\nu} = 1545$ and 1640 cm^{-1} can be assigned to pyridinium-ion ring vi-

Table 1. Acid density information from quantitative analysis of the NH_3 -TPD and Py-IR results.

Sample	Total acid amount from NH_3 -TPD [mmol g^{-1}]	Acid amount from Py-IR		
		Brønsted acid sites [au]	Lewis acid sites [au]	B/L ratio
SBA-15	0.01	0	0	–
M-AS-30	0.17	122	554	0.22
C-AS-30	0.30	170	581	0.29
W-AS-30	0.37	181	659	0.27
N-AS-30	0.40	362	654	0.55
$\gamma\text{-Al}_2\text{O}_3$	0.32	0	645	–
6Mo/SBA-15	0.04	0	786	–
6Mo/M-AS-30	0.32	224	423	0.53
6Mo/C-AS-30	0.38	283	449	0.63
6Mo/W-AS-30	0.37	292	497	0.59
6Mo/N-AS-30	0.40	411	583	0.70
6Mo/ $\gamma\text{-Al}_2\text{O}_3$	0.30	173	632	0.27

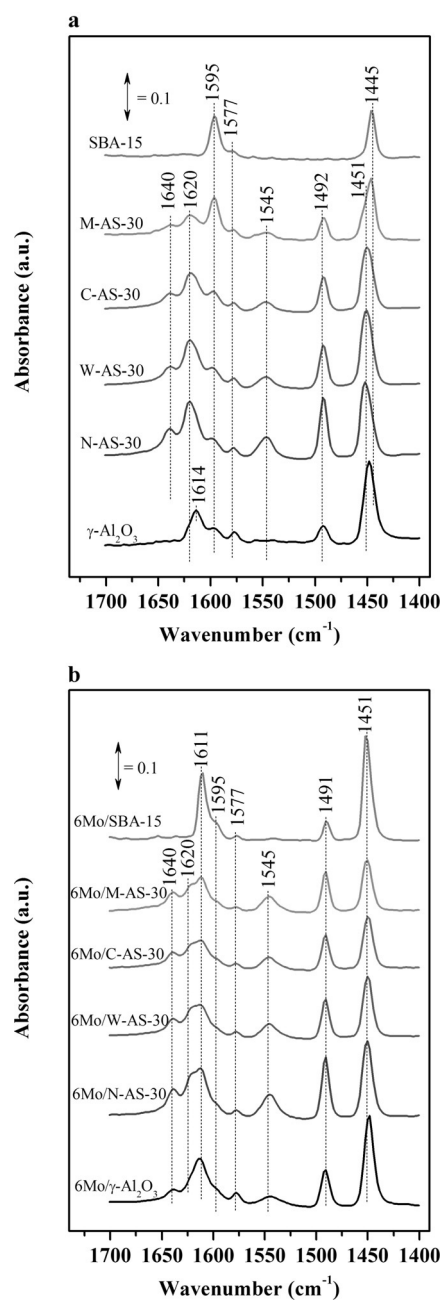


Figure 6. IR spectra of pyridine adsorbed on a) alumina premodified composite samples and b) the corresponding Mo-based catalysts after evacuation at 150°C for 0.5 h.

brations resulting from proton transfer from the Brønsted acid sites to pyridine. The band at $\tilde{\nu}=1492\text{ cm}^{-1}$ is ascribed to pyridine associated with both Lewis and Brønsted acid sites. As to pristine SBA-15, only two intense bands at $\tilde{\nu}=1445$ and 1595 cm^{-1} are detected, which indicates that neither Lewis nor Brønsted acid sites exist on pristine SBA-15. As far as the $\gamma\text{-Al}_2\text{O}_3$ support is concerned, the presence of bands at $\tilde{\nu}=1448$, 1492 , 1575 , and 1614 cm^{-1} demonstrates the existence of Lewis acid sites. Furthermore, no band at approximately $\tilde{\nu}=1545\text{ cm}^{-1}$ corresponding to the Brønsted acid sites is observed, which indicates that the surface hydroxy groups on $\gamma\text{-Al}_2\text{O}_3$ are not strong enough to protonate the pyridine molecules.^[44] In the spectra of the alumina-modified SBA-15 samples, new bands at $\tilde{\nu}=1545$ and 1640 cm^{-1} corresponding to Brønsted acid sites are observed, which may confirm the formation Si–O(H)–Al linkages. On the basis of quantitative analysis of the Py-IR results (listed in Table 1), introducing alumina on SBA-15 could generate both new Brønsted and Lewis acid sites, and the number of Brønsted acid sites decreases in the following order: N-AS-30 > W-AS-30 > C-AS-30 > M-AS-30.

Moreover, the ratio of Brønsted acid sites to Lewis acid sites (B/L ratio) decreases in the same order. The higher B/L ratio of N-AS-30 demonstrates that more Al atoms are transformed into the Si–O–Al framework structures. This order is also in good agreement with the band intensity of the silanol groups in the hydroxy region (Figure 5), that is, the higher the number of Brønsted acid sites, the lower the band intensity of the silanol groups. On the basis of these results, we could confirm that the relative interaction between the alumina guest and the SBA-15 host is strongly dependent on the method used to introduce the alumina. Introducing alumina by the NIH method was more favorable for the interaction of the oxygen atoms of the silanol groups with the neighboring Al atoms, and this left fewer free silanol groups. As a result, more Si–O(H)–Al framework structures and Brønsted acid sites were formed over N-AS-30. Careful investigation of the band at $\tilde{\nu}=1595\text{ cm}^{-1}$ of pristine SBA-15 to that of the alumina-modified SBA-15 samples also revealed some critical information. Specifically, the intensity of this band for M-AS-30 decreased only slightly relative to that of pristine SBA-15, and moreover only a weak band at $\tilde{\nu}=1545\text{ cm}^{-1}$ was observed. With respect to N-AS-30, the intensity of the band at $\tilde{\nu}=1595\text{ cm}^{-1}$ greatly decreased, and much more Brønsted acid sites were generated. Combined with the N_2 adsorption/desorption isotherms and the TEM results, it is evident that most of the alumina accumulates outside the mesopores if the MG method is used.

Characterization of the Mo-based catalysts

The pore structure of the Mo-based catalysts was investigated by N_2 adsorption/desorption isotherms and low-angle XRD measurements (Figure S3 and Figure 7a). All the catalysts (except for Mo/ $\gamma\text{-Al}_2\text{O}_3$) exhibit a typical mesoporous structure similar to that of the corresponding supports, which indicates that loading the Mo species does not destroy the mesostructure of the supports. Furthermore, the specific surface area decreased as expected. Relative to that of Mo/SBA-15, the de-

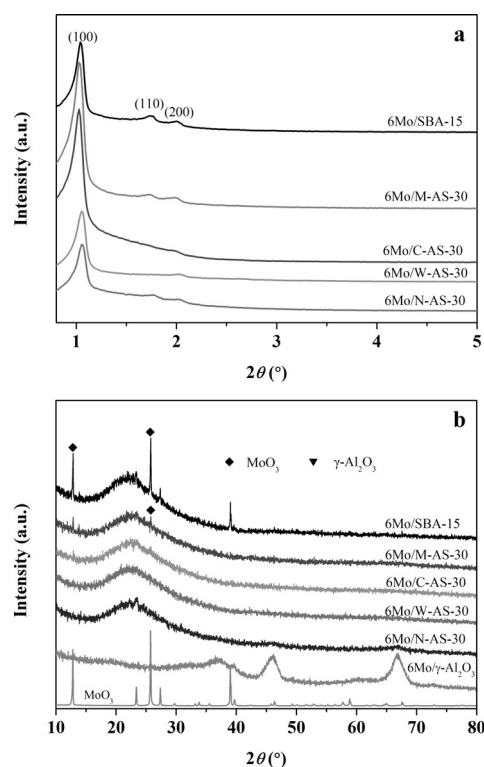


Figure 7. a) Low-angle and b) wide-angle XRD patterns of Mo-based catalysts supported on the pristine SBA-15, $\gamma\text{-Al}_2\text{O}_3$, and alumina premodified composite samples.

crease in the specific surface area for the four alumina-modified catalysts was more pronounced, and among these, Mo/N-AS-30 possessed the highest value of $296\text{ m}^2\text{ g}^{-1}$ (Figure S3). Great difference was observed in the wide-angle XRD patterns of the Mo-based catalysts (Figure 7b). Diffraction peaks of crystalline MoO_3 were observed for Mo/SBA-15 owing to the weak interaction between the SBA-15 parent and the Mo species, whereas no diffraction peaks of crystalline MoO_3 could be observed for Mo/C-AS-30, Mo/W-AS-30 and Mo/N-AS-30; this indicated that the loaded Mo species were highly dispersed on these composite supports as amorphous Mo species or existed as MoO_3 crystallites too small to be detected by XRD.^[45] On the contrary, the diffraction peaks for crystalline MoO_3 were still visible for Mo/M-AS-30, and this implies a lower dispersion of Mo species over the M-AS-30 support. This conclusion was further proved by Raman spectroscopy through the presence of characteristic bands (e.g. $\tilde{\nu}=994$, 818 , and 665 cm^{-1}) resulting from crystalline MoO_3 ^[46] for Mo/SBA-15 and Mo/M-AS-30 (Figure S4).

The chemical compositions of the Mo-based catalysts are summarized in Table 2. According to the X-ray fluorescence spectrometry (XRF) results, the overall Mo contents of these samples were approximately 6 wt%, except for Mo/SBA-15. The bulk Si/Al ratios were in good agreement with the nominal values. On the basis of the XPS results, the surface Si/Al ratios exhibited great differences depending on the alumina coating method. The lowest value was observed on the well-coated Mo/N-AS-30 sample, whereas Mo/M-AS-30 possessed the high-

Table 2. Chemical compositions of the Mo-based catalysts supported on the pristine SBA-15, γ -Al₂O₃, and alumina premodified composite samples.

Sample	Bulk (XRF)		Surface (XPS)		
	Mo loading [wt %]	Si/Al [mol/mol]	Si/Al ^[a] [mol/mol]	Mo/Si ^[b] [mol/mol]	Mo/(Si + Al) ^[c] [mol/mol]
Mo/ γ -Al ₂ O ₃	5.6	–	–	–	0.039
Mo/N-AS-30	5.8	2.1	1.2	0.072	0.040
Mo/W-AS-30	6.3	2.0	1.9	0.057	0.037
Mo/C-AS-30	5.9	2.1	2.5	0.042	0.030
Mo/M-AS-30	5.5	2.7	4.4	0.037	0.030
Mo/SBA-15	4.8	–	–	0.020	–

[a] The surface atomic ratio of Si to Al. [b] The surface atomic ratio of Mo to Si. [c] The surface atomic ratio of Mo to (Si + Al).

est value. This phenomenon was supposed to be related to the distribution of aluminum, and the alkaline environment may assist migration and dispersion of the Al species over pristine SBA-15. In addition, the surface Mo/Si and Mo/(Si + Al) ratios of the catalysts increased in the reverse order of the surface Si/Al ratio, and Mo/N-AS-30 possessed the highest value, which demonstrates that the distribution of Mo species parallels that of the Al species on the support. Consequently, interaction of the Mo species with the alumina component was preferred to that with SBA-15. Good dispersion of alumina inside the SBA-15 channel may guarantee the good distribution of Mo species on the catalyst. Li et al. also observed the preferential distribution of Mo on alumina on the H β -Al₂O₃ support.^[47] In addition, the formed bridging hydroxy groups may be beneficial to the dispersion of Mo species on the composite support.

Time-of-flight secondary-ion mass spectrometry (TOF-SIMS) was employed to further investigate the surface states of the Mo species. This technique is particularly helpful in understanding the mutual interactions between the interatoms and analyzing the outermost surface compositions of the heterogeneous catalysts.^[25,26,48,49] Here, more attention was focused on the Mo dispersion in terms of fragments containing one or more Mo atoms (i.e., MoO_x⁻, Mo₂O_x⁻, and Mo₃O_x⁻). As shown in Figure 8, the fragments containing one or more Mo atoms were all observed on the prepared Mo-based catalysts, and this is indicative of the presence of both isolated MoO_x species and polymeric molybdates. It is clear that Mo/SBA-15 exhibited largely polymeric Mo species, and the ratio of “poly-Mo/(poly-Mo + mono-Mo)” was as high as 49.3%. The value decreased to only 2.5% for Mo/ γ -Al₂O₃, which was due to the stronger interaction of the Mo species with the γ -Al₂O₃ support. As a result, the majority of Mo species was highly dispersed as monomeric Mo species. With respect to the Mo-based catalysts supported on alumina-modified SBA-15, the ratio was 6.2 and 9.1% for Mo/N-AS-30 and Mo/M-AS-30, respectively, and this indicated that the degree of dispersion of the Mo species was much higher if the composite support was prepared by the NIH method. In addition, these ratios are only slightly higher than that of Mo/ γ -Al₂O₃ but are remarkably lower than that of Mo/SBA-15. This result revealed the advantageous function of alumina for enhancing the dispersion of Mo species.

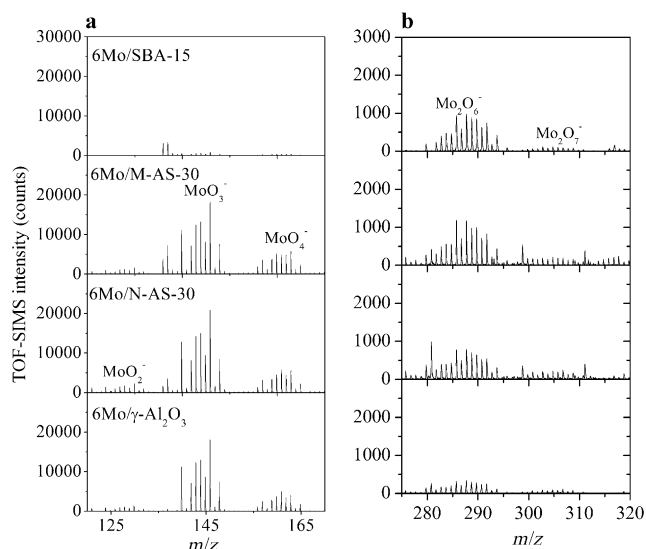


Figure 8. Partial negative TOF-SIMS spectra of the Mo-based catalysts a) in the $m/z = 120$ – 170 range corresponding to monomeric Mo clusters and b) in the $m/z = 275$ – 320 range corresponding to dimeric Mo clusters. The fragments with one Mo atom are denoted as “mono-Mo” clusters, whereas those containing more than one Mo atoms are denoted as “poly-Mo” clusters.^[26,50]

The NH₃-TPD profiles of the Mo-based catalysts are presented in Figure 9. It was found that the Mo loading did not clearly alter the overall shape of the TPD peak, but the total amount of acid changed greatly depending on the corresponding supports (Table 1). Mo/SBA-15 showed a small NH₃ desorption peak, which indicated that new acid sites were formed after loading Mo species on SBA-15. An increase in the total amount of acid was also observed for Mo/M-AS-30 and Mo/C-AS-30, whereas the total amount of acid for Mo/W-AS-30 and Mo/N-AS-30 was almost the same as that of their corresponding supports. It is well known that the reactivity of transition-metal ions with supports depends on the type of surface hydroxy groups or acid sites. For example, as far as Re₂O₇/ γ -Al₂O₃ catalysts are concerned, the rhenium ions predominately react with basic hydroxy groups at low Re contents, whereas they also react with neutral and more acidic hydroxy groups at

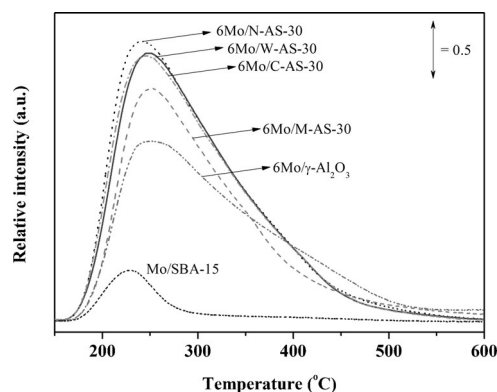


Figure 9. NH₃-TPD profiles of the Mo-based catalysts supported on the pristine SBA-15, γ -Al₂O₃, and alumina premodified composite samples.

higher Re loadings.^[51] From quantitative analysis of the Py-IR results (Table 1), loading of the Mo species decreased the number of Lewis acid sites, whereas it increased the number of Brønsted acid sites (except for Mo/SBA-15), which indicated that new Brønsted acid sites related to Mo species were generated. As a result, the B/L ratio of the catalysts increased relative to that of the corresponding supports. Particularly, no Brønsted acid sites could be observed on the pure γ -Al₂O₃ support, whereas they appeared after loading the Mo species, and this is in agreement with recently published work.^[52] The formed surface Mo–OH and Mo–O(H)–Si/Al groups may be the origin of the newly generated Brønsted acid sites. On the whole, the amount of Brønsted acid sites decreased in the order: Mo/N-AS-30 > Mo/W-AS-30 > Mo/C-AS-30 > Mo/M-AS-30 > Mo/ γ -Al₂O₃. This is in full conformity with order of the supports.

The effects of the way in which alumina was introduced on the reducibility of the Mo species were investigated by temperature-programmed reduction of H₂ (H₂-TPR) experiments. As shown in Figure 10, Mo/SBA-15 started to be reduced at approximately 500 °C, and it progressively continued until 900 °C. The broadening signal contains three reduction peaks centered at $T=592, 778$ and 895 °C. Two characteristic reduction peaks centered at $T=436$ and 900 °C were observed on Mo/ γ -Al₂O₃. Relative to that observed for Mo/SBA-15 and Mo/ γ -Al₂O₃, there was a great change in the reduction behavior of the Mo-based catalysts supported on the alumina-modified SBA-15 sample as a result of changes in the properties of the support. The most significant change in the H₂-TPR profile was the emergence of a broad peak at $T=720$ – 780 °C; this change was accompanied by the formation of a shoulder peak at approximately $T=900$ °C, which was distinct for Mo/SBA-15 and Mo/ γ -Al₂O₃. As reported by Klimova et al.,^[43] a new reduction peak appeared for Mo-based catalysts supported on Al-containing SBA-15 after aluminum incorporation into SBA-15, whereas the higher temperature peak was still legible. The disparity between the present work and that of Klimova et al. may result from different alumina contents in modified SBA-15. With respect to the zirconia-modified SBA-15 support, the intensity of the higher temperature reduction peak of the Mo species also markedly decreased, and this was accompanied by an increase in the lower temperature peak.^[18] Combined with the Py-IR results,

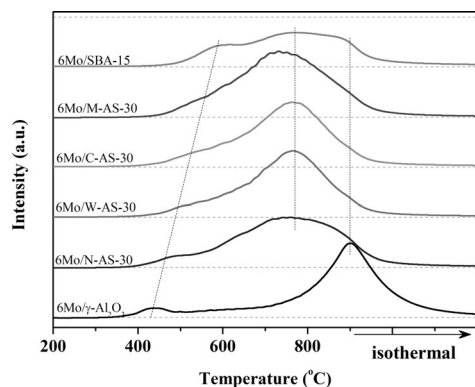


Figure 10. H₂-TPR profiles of the Mo-based catalysts supported on the pristine SBA-15, γ -Al₂O₃, and alumina premodified composite samples.

we speculate that the broad peak at $T=720$ – 780 °C is primarily related to the Brønsted acid sites on the composite support. This assumption is also supported by our previous study concerning the H₂-TPR profiles of the Mo/ β -Al₂O₃ metathesis catalyst.^[53] As to the lower temperature reduction peak between $T=430$ and 600 °C, the peak temperature increased in the order: Mo/ γ -Al₂O₃ < Mo/N-AS-30 < Mo/W-AS-30 < Mo/C-AS-30 < Mo/M-AS-30 < Mo/SBA-15. Thus, it is clear that introduction of alumina into pristine SBA-15 changes the interaction between the Mo species and the supports. The newly formed bridging hydroxy groups are favorable for the reduction of highly dispersed Mo species.

Catalytic performance of the Mo-based catalysts

The effect of different reaction temperatures

First, the 1-butene metathesis reaction at different temperatures over Mo/SBA-15, Mo/ γ -Al₂O₃, Mo/W-AS-30, and Mo/N-AS-30 was evaluated, and the results are presented in Figure 11. The catalyst activity and product yield were strongly dependent on the reaction temperature. Notably, the Mo/SBA-15 catalyst exhibited poor metathesis activity and propene yield at temperatures below 250 °C. Both butene conversion and propene yield increased with increasing temperature. Notably, the molar ratio of 2-butene to 1-butene was already higher than 1.0 in the product at 250 °C (Figure 11 a). This was an indication that a high temperature was a requisite for metathesis I (Scheme 1) over Mo/SBA-15. The yield of ethene also slightly increased with increasing temperature, but the yield was lower than 3% in the temperature region investigated in this work. Only a trace amount of isobutene was observed even at 440 °C, which is indicative of the low acidity of the Mo/SBA-15 catalyst, and this is in agreement with the above NH₃-TPD result and results reported in Ref. [54].

Mo/ γ -Al₂O₃ showed better performance than Mo/SBA-15 at low temperatures. At 120 °C, the yield of ethene was 11.4%, whereas the yield of propylene was only 10.2%; this indicated that the self-metathesis of 1-butene dominated in the metathesis reactions and that metathesis I was suppressed owing to the low molar ratio of 2-butene to 1-butene in the product [$n(2-C_4^=)/n(1-C_4^=)=0.1$].^[55] The conversion of butene reached a maximum of 65.6% at 180 °C, whereas the highest yield of propene of 27.6% was obtained at a temperature of 210 °C (Figure 11 b). In addition, the yield of ethene gradually diminished upon increasing the reaction temperature. This may be due to the increased isomerization activity of 1-butene to 2-butene [as confirmed by the increased value of $n(2-C_4^=)/n(1-C_4^=)$ with temperature], which was not beneficial for metathesis II (Scheme 1).^[14,56]

The introduction of alumina species into pristine SBA-15 during the preparation of the supports showed a strong impact on the catalytic performance of the prepared Mo-based catalysts. As shown in Figure 11 c, the Mo/W-AS-30 catalyst already exhibited certain metathesis activity at 60 °C, and the conversion of butene and the yield of propene were 36.3 and 12.2%, respectively. The yield of propene increased with increasing temperature, and it reached a maximum of 27.3% at

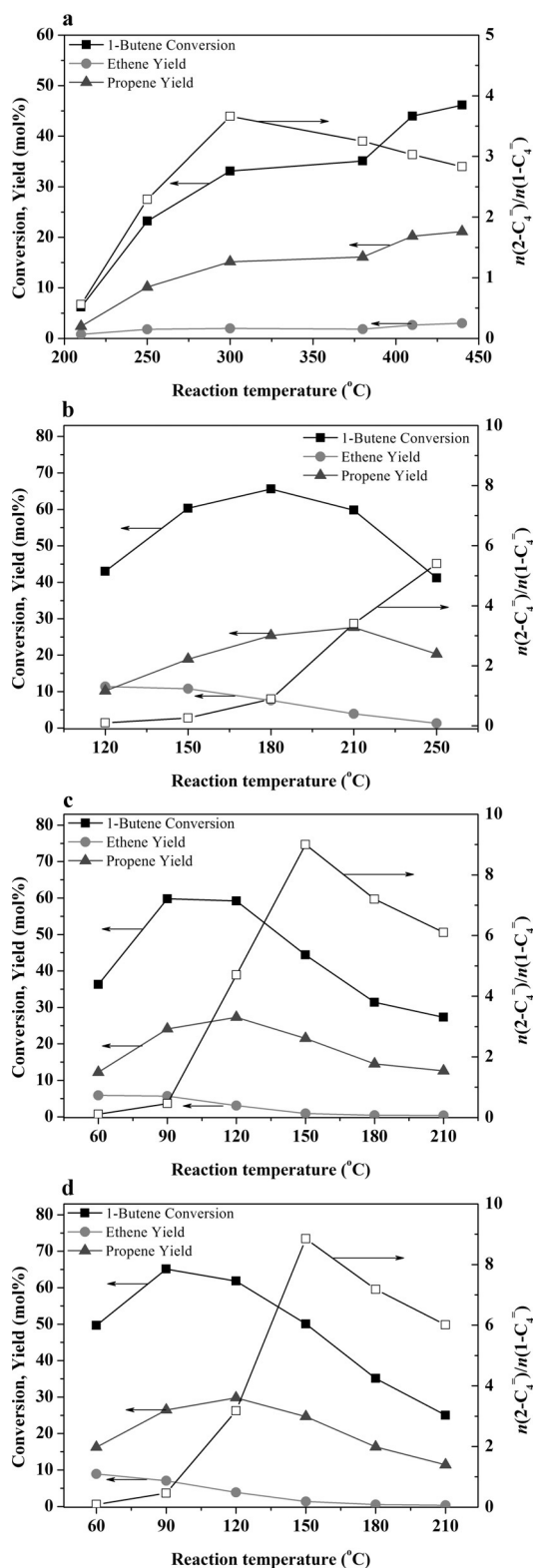


Figure 11. Temperature dependence of the catalytic performance on the a) Mo/SBA-15, b) Mo/ γ -Al₂O₃, c) Mo/W-AS-30, and d) Mo/N-AS-30 catalysts. (Reaction pressure: 0.1 MPa, WHSV: 1.5 h⁻¹, time on stream: 1 h).

120 °C. Both the conversion of butene and the yield of propene decreased upon increasing the temperature further, and they decreased to 27.3 and 12.6%, respectively, at 210 °C. Simi-

lar catalytic behavior was observed on Mo/N-AS-30. To be specific, two volcano-shaped patterns were found with respect to the conversion of butene and the yield of propene as a function of reaction temperature. The maximum yield of propene of 29.8% was also found at 120 °C, and this is slightly higher than that found on Mo/W-AS-30. Notably, the metathesis activity of Mo/N-AS-30 was better than that of Mo/W-AS-30 at lower temperature (i.e., 60–120 °C), whereas as the activity decreased with increasing temperature (120–210 °C), and the decreasing trend was clearer for Mo/N-AS-30. Particularly, the conversion of butene and the yield of propene on Mo/N-AS-30 decreased to 25.0 and 11.4%, respectively, at 210 °C, and these values are lower than those on Mo/W-AS-30. According to the Py-IR results and H₂-TPR measurements, the number of Brønsted acid sites on Mo/N-AS-30 was higher than that on Mo/W-AS-30. This would facilitate reduction of the Mo species to metal-carbene intermediates by the olefin at a relatively lower temperature. Recently, Amakawa et al.^[57] confirmed the importance of Brønsted acidity (originating from the molybdenol groups) on Mo-based catalysts supported on SBA-15. They postulated that the Brønsted hydroxy groups protonate the olefin reactant to form an intermediate species, which is further converted into the metathesis-active Mo-alkylidene species. Therefore, it is reasonable that preferable metathesis activity was observed on Mo/N-AS-30, whereas deep reduction of Mo species may occur under the influence of Brønsted acid sites if the reaction temperature is higher, and this is not beneficial for the olefin metathesis reaction.^[58,59] It is generally accepted that highly isolated Mo species are the active precursors for olefin metathesis.^[26,60] Although Mo/ γ -Al₂O₃ exhibits numerous isolated Mo species, poor metathesis activity was observed at 120 °C owing to a low number of acid sites. Higher metathesis activity and product yields were obtained over Mo/N-AS-30 and Mo/W-AS-30, which benefit from a sufficient number of acid sites and well-dispersed Mo species on these catalysts. On the whole, introducing alumina onto/into pristine SBA-15 take advantages of both mesoporous SBA-15 and traditional alumina, and synergetic effects occur inside the composite supports in term of Mo dispersion and the low-temperature metathesis reaction. Indeed, this method can be used for the preparation of effective metathesis catalysts. Therefore, we subsequently investigated the effects of the method of introduction of alumina, that is, NIH, WIH, CI, and MG, on the activity of the final catalysts in the metathesis of 1-butene.

The effect of the method of introduction of alumina

The catalytic performance of 1-butene metathesis over the as-prepared Mo-based catalysts with different methods for the introduction of alumina are presented in Table 3 and Figure S5. Similar metathesis activity and product distributions were observed at 1 h on stream. The butene conversions were in the range of 56 to 62%, and Mo/N-AS-30 exhibited the highest conversion. The main metathesis products were propene (26–30%) and pentene (18–20%), with ethene (2–4%) and hexene (6–7%) in relatively lower proportions. These results indicate that metathesis I was the primary metathesis reaction, whereas

the self-metathesis of 1-butene (metathesis II) contributed less to the overall reaction. Generally, the double bond isomerization step of 1-butene to 2-butene is fast relative to the metathesis steps over more acidic catalysts,^[54] and this reaction may be limited by its thermodynamic equilibrium and is favorable for the formation of 2-butene with a relatively higher ratio of 2-butene to 1-butene at 120 °C (in the range of 3.2 to 5.7, as listed in Table 3).^[13] Consequently, it is understandable that metathesis I should take place predominately over the catalysts. Moreover, if propene and pentene were mainly produced through metathesis I, the stoichiometric ratio of $n(C_3^-)/n(C_5^-)$ should be equal to 1.0. In fact, it was above 1.0, that is, the yield of propene was higher than that of its co-product pentene, because of the contribution of metathesis III (Scheme 1). This was also verified by the fact that the yield of ethene was lower than that of hexene. Meyer et al.^[56] performed thermodynamic calculations, and they also found that the theoretical yield of propene was higher than that of pentene by using a mixture of 1-butene and 2-butene as feed.

The conversion of butene and the product distribution after 28 h on stream are also included in Table 3. It can be seen that the metathesis stability is highly dependent on the method of introduction of alumina. The conversion of butene and the yield of propene on Mo/M-AS-30 dropped from 57.6 to 17.7% and from 26.9 to 8.5%, respectively, after 28 h on stream. To be specific, the Mo/M-AS-30 catalyst underwent a faster deactivation rate of 1.23% h⁻¹ within the first 10 h (Figure 12), and after this period, the deactivation rate slowed down. Anyway, this catalyst showed the lowest yield of propene after 28 h on stream, and the corresponding percent yield of propene decreased by 68.4% relative to that obtained after 1 h (Table 3). The Mo/N-AS-30 catalyst exhibited the best stability among the tested Mo-based catalysts, and it was even more stable than the previously reported Mo/HMOR-Al₂O₃ catalyst under the same reaction conditions.^[61] The yield of propene was still as high as 23.1% after 28 h on stream, and the percent yield decreased by 22.5% relative to that obtained after 1 h. Moreover, the profile of the yield of propene on Mo/N-AS-30 was approximately linear with a deactivation rate of 0.25% h⁻¹

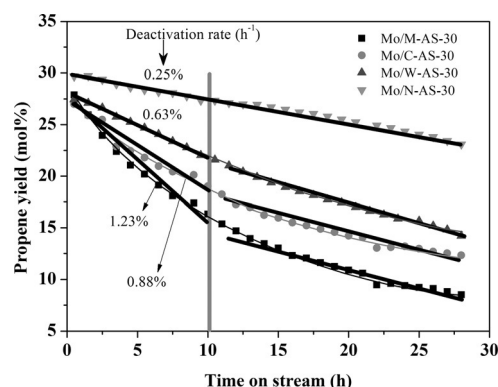


Figure 12. Deactivation rate of Mo-based catalysts supported on alumina premodified composite samples in terms of propene yield. (Reaction temperature: 120 °C, reaction pressure: 0.1 MPa, WHSV: 1.5 h⁻¹)

during the reaction period (Figure 12), and this value is much lower than that on Mo/M-AS-30. Propene yields of 12.3 and 14.2% were obtained over Mo/C-AS-30 and Mo/W-AS-30, respectively; these yields are higher than the yield over Mo/M-AS-30 but lower than the yield over Mo/N-AS-30. For all catalysts, the yields of ethene and hexene from metathesis II also decreased with time on stream, and still, the Mo/N-AS-30 catalyst showed the highest yields of ethene and hexene at 28 h on stream, which implies that both metathesis I and metathesis II were highly active on Mo/N-AS-30. As discussed above, alumina introduced by the NIH method is highly dispersed on the pore walls, and the well-defined mesopores of the SBA-15 host are preserved. Moreover, many more Brønsted acid and active metathesis Mo species were formed on Mo/N-AS-30. As a result, a much lower deactivation rate was observed. Consequently, the effective synergy of alumina and SBA-15 in light of the metathesis stability was realized only if the NIH method was employed. As to Mo/M-AS-30, the majority of alumina accumulated outside the channels, and this was detrimental to host-guest interactions and to the dispersion of the Mo species. Thus, it is reasonable that Mo/M-AS-30 exhibited poor metathesis stability. The interaction of the alumina guest and

Table 3. Product distribution over the Mo-based catalysts at various stages in the 1-butene metathesis reaction.^[a]

Catalyst	Conversion [mol%]	Yield [mol%]					Mole ratio of the product [mol/mol]			
		C ₂ ⁼	C ₃ ⁼	C ₅ ⁼	C ₆ ⁼	C ₇ ⁺	$n(2-C_4^-)/n(1-C_4^-)$	$n(C_3^-)/n(C_5^-)$	$n(C_2^-)/n(C_6^-)$	
Time on stream: 1 h										
Mo/M-AS-30	57.6	2.6	26.9	19.8	6.2	2.0	3.9	1.4	0.42	
Mo/C-AS-30	56.1	2.4	26.4	19.0	6.0	2.1	5.7	1.4	0.40	
Mo/W-AS-30	59.2	3.1	27.3	19.5	6.8	2.4	4.7	1.4	0.45	
Mo/N-AS-30	61.8	3.8	29.8	18.4	6.9	2.7	3.2	1.6	0.55	
Time on stream: 28 h										
Mo/M-AS-30	17.7	0.4	8.5 (68.4) ^[b]	7.6	0.9	0.4	4.7	1.1	0.44	
Mo/C-AS-30	25.7	0.6	12.3 (53.4) ^[b]	10.7	1.5	0.5	6.1	1.1	0.40	
Mo/W-AS-30	30.0	0.8	14.2 (48.0) ^[b]	12.3	2.1	0.5	5.7	1.2	0.38	
Mo/N-AS-30	47.0	1.4	23.1 (22.5) ^[b]	17.6	3.9	1.0	8.1	1.3	0.36	

[a] Reaction temperature: 120 °C, reaction pressure: 0.1 MPa, WHSV: 1.5 h⁻¹. [b] Number in parentheses is the decrease in the percent yield of propene after 28 h on stream relative to that after 1 h.

the SBA-15 host is stronger in Mo/W-AS-30 and Mo/C-AS-30 than in Mo/M-AS-30, whereas blockage of the mesopore channel was found by the accumulated alumina species. This would also influence molecular diffusion and catalytic stability to some extent.

Unlike the varied trends of the metathesis products, the molar ratio of 2-butene to 1-butene increased, especially for Mo/N-AS-30.^[14] One possible reason is the gradual decay of metathesis III; as a result, the content of 2-butene increases to a higher level with time on stream. As far as Mo/N-AS-30 is concerned, the molar ratio of 2-butene to 1-butene was the highest after 28 h on stream, and thus, the lowest deactivation rate of metathesis I on Mo/N-AS-30 could not be excluded. On the whole, the ratio of 2-butene to 1-butene remained above 3.0 during the reaction period, which indicated that double-bond isomerization was not the critical factor leading to catalyst deactivation.

Variations in the product yield with butene conversion are presented in Figure 13. The yield of each product seems to depend on butene conversion following a similar trend. The yield of propene increased linearly with the conversion of butene, irrespective of the catalyst, and this is indicative of constant propene selectivity during the reaction. Additionally, the most selective product was propene, especially at higher butene conversions. The steady yield of propene upon Mo/N-AS-30 was due to its higher catalytic activity. Interestingly, the yield of pentene initially increased with the conversion of butene, similar to that observed for propene. Nevertheless, it exhibited a maximum if the conversion was higher than 45%. As shown in Scheme 1, pentene was primarily produced from metathesis I, with propene as a coproduct. Propene could also be produced through metathesis III followed by metathesis II. Therefore, it is speculated that metatheses I, II, and III exhibit high reactivity at high conversions of butene. This could be further proved by the observation that the yields of both ethene and hexene presented an approximately exponential increase if the conversion of butene was higher than 40%. Although the deactivation rates of the three Mo-based catalysts were different, the product yields of ethene, propene, pentene, and hexene as a function of the conversion of butene followed similar trends. This gave us some indication that there existed

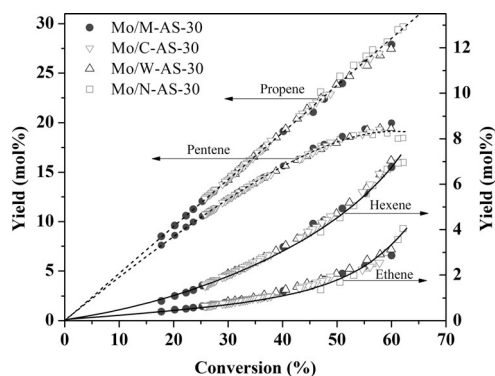


Figure 13. Variation in the product yields with butene conversion over the Mo/M-AS-30, Mo/W-AS-30, and Mo/N-AS-30 catalysts.

great consistency between the mechanisms of both the metathesis reaction of 1-butene and its deactivation over these catalysts, irrespective of the method used to introduce alumina.

Carbonaceous deposits on active metathesis sites were critical factors leading to catalyst deactivation; their formation was mainly caused by olefin oligomerization, which was generally associated with the acid sites.^[58,61] To analyze the carbonaceous species deposited on the spent catalysts, an oxygen temperature-programmed oxidation (O₂-TPO) experiment was performed. As shown in Figure 14, all of the spent catalysts exhibited mainly two burning peaks at the same temperatures (358 and 476 °C), which indicated that the deposited carbonaceous species possessed similar properties. Interestingly, the integral area of all peaks increased in the order: Mo/N-AS-30 > Mo/W-AS-30 > Mo/C-AS-30 > Mo/M-AS-30, which correlates well with the catalyst stability. Thus, the amount of carbonaceous deposits on the catalysts was not directly related to the metathesis stability, as Mo was the metathesis-active site. On basis of the above results, it was concluded that the high dispersion of Mo species and the well-defined mesostructure of N-AS-30 guarantee high accommodation coke capacity of Mo/N-AS-30 and good metathesis stability in the reaction.

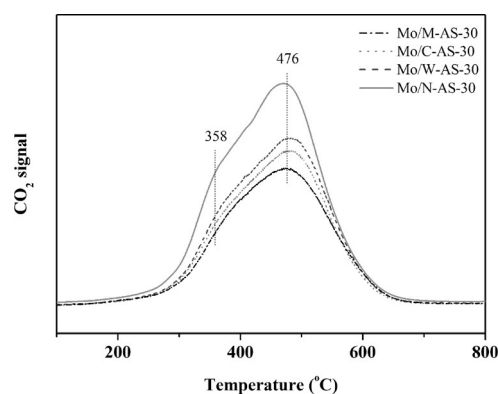


Figure 14. O₂-TPO profiles of the spent Mo/M-AS-30, Mo/C-AS-30, Mo/W-AS-30, and Mo/N-AS-30 catalysts.

Conclusions

In this study, four Al₂O₃-SBA-15 composite supports with different alumina location states were prepared through postsynthesis methods, that is, ammonia/water vapor induced hydrolysis, water vapor induced hydrolysis, conventional impregnation, and mechanical grinding. The corresponding Mo-based catalysts were evaluated in the autometathesis of 1-butene. It was found that the dispersion of the Mo species and the metathesis activity and stability were closely associated with the location states of guest alumina on the SBA-15 host, which was strongly dependent on the modification methods of SBA-15 with alumina.

Upon using the mechanical grinding method, most of the alumina accumulated outside the mesopore channels. Water vapor induced hydrolysis and the conventional impregnation method led to blockage of the mesopores to some extent

with the introduction of alumina. Well-dispersed alumina on the mesopore walls of SBA-15 was realized without pore-channel blocking by using the ammonia/water vapor induced hydrolysis (NIH) method. In fact, a better combination of guest alumina and host SBA-15 was realized by the NIH method through the formation of Si–O(H)–Al hydroxy groups.

It was found that the Mo species preferentially interacted with alumina and not siliceous SBA-15. A uniform distribution of alumina around the SBA-15 channel guaranteed the high dispersion of the Mo species on the support. Moreover, the generation of new Brønsted acid sites was also favorable for dispersion of the Mo species and low-temperature butene metathesis activity. The optimal reaction temperature for the metathesis of butene was related to the number of Brønsted acid sites. In general, a novel Mo-based catalyst with a Al_2O_3 @SBA-15 composite support prepared by the NIH method exhibited the best metathesis activity and stability among the tested catalysts under the reaction conditions of 120 °C, 0.1 MPa, and weight hourly space velocity = 1.5 h⁻¹ as a result of its good Mo dispersion and high Brønsted acid density.

Experimental Section

Coating alumina on SBA-15

Commercial mesoporous SBA-15 was supplied by Novel Chemical Technology Corporation and was calcined at 500 °C before use. Alumina was introduced into the SBA-15 host by four different methods, namely, ammonia/water vapor induced hydrolysis (NIH),^[30,62] water vapor induced hydrolysis (WIH), conventional impregnation (CI), and mechanical grinding (MG), in which $\text{Al}(\text{NO}_3)_3 \cdot 9\text{H}_2\text{O}$ was used as the source of alumina. Iengo et al.^[63] reported that the amount of aluminum required to create an Al monolayer coverage on silica with a surface area of 280 m²g⁻¹ was 2.1 mmol g⁻¹, which corresponds to a surface concentration of 7.5 μmol m⁻². The surface area of SBA-15 used herein was 532 m²g⁻¹. Therefore, approximately 30 wt% of alumina coating was employed on SBA-15 in this work by different methods to obtain an Al coverage higher than its monolayer.

Alumina coating onto/into SBA-15 by the NIH method was performed by following a reported procedure.^[30] Typically, mesoporous SBA-15 (1.0 g) was dispersed in a 10 mL aqueous solution of $\text{Al}(\text{NO}_3)_3 \cdot 9\text{H}_2\text{O}$ (1.58 g). The mixture was then evaporated at 60 °C until dryness, which was followed by drying at 100 °C for 6 h. To improve the dispersion of alumina inside the pores, this impregnation step was repeated once more, which allowed an alumina loading of 30 wt% to be obtained. Subsequently, the Al-precursor-loaded SBA-15 was put in an open container made of Teflon, and then kept in an autoclave containing a $\text{NH}_3/\text{H}_2\text{O}$ solution with no direct contact between the solid and solution. The tightly closed autoclave was then heated to 100 °C for 7 h. After treatment, the solid was dried at room temperature for 6 h and then at 100 °C for 12 h. Finally, the material was calcined at 500 °C for 5 h in air, and the obtained composite support is denoted N-AS-30. The procedure for the WIH method was similar to that for the NIH method, except that the liquid in the autoclave was deionized water, and the resultant material is denoted W-AS-30. For the conventional impregnation method, alumina-loaded SBA-15 was directly calcined at 500 °C for 5 h without $\text{NH}_3/\text{H}_2\text{O}$ vapor treatment, and the

resultant support is denoted C-AS-30. As to the solvent-free grinding method, $\text{Al}(\text{NO}_3)_3 \cdot 9\text{H}_2\text{O}$ (3.16 g) was manually ground together with SBA-15 (1.0 g) in a mortar at room temperature for 0.5 h. The obtained powder was calcined at 500 °C for 5 h in air and is denoted M-AS-30.

Catalyst preparation

Catalysts containing approximately 6.0 wt% Mo were prepared by incipient wetness impregnation of the composite supports with an aqueous solution of $(\text{NH}_4)_6\text{Mo}_7\text{O}_{24} \cdot 4\text{H}_2\text{O}$ and left at room temperature for 24 h. The concentration of ammonium molybdate depended on the quantity and water absorbability of the support. The samples were then dried at 120 °C for 4 h and finally calcined at 600 °C for 2 h. The final catalysts are denoted Mo/N-AS-30, Mo/W-AS-30, Mo/C-AS-30, and Mo/M-AS-30 for Mo species supported on N-AS-30, W-AS-30, C-AS-30, and M-AS-30, respectively. For comparison, Mo-based catalysts supported on $\gamma\text{-Al}_2\text{O}_3$ and SBA-15, respectively, were also prepared.

Catalysts characterization

The N_2 adsorption/desorption isotherms measurements were performed at -196 °C with a Micromeritics ASAP 2020 instrument. X-ray diffraction (XRD) patterns were collected with an X'Pert PRO diffractometer. Transmission electron microscopy (TEM) images were obtained with an FEI Tecnai G2 Spirit microscope with an acceleration voltage of 100 kV. ²⁷Al NMR spectra were measured with a Bruker AVANCE 500 spectrometer. Diffuse reflectance infrared Fourier transform spectroscopy (DRIFTS) experiments in the hydroxy region were performed with a Bruker VERTEX 70 spectrometer equipped with a Harrick Praying Mantis optical accessory. Infrared spectroscopy of adsorbed pyridine (Py-IR) was used to differentiate between Lewis and Brønsted acid sites. Temperature-programmed desorption of ammonia (NH_3 -TPD) and temperature-programmed reduction of H_2 (H_2 -TPR) experiments were performed in a quartz microreactor (i.d. 4 mm) that was connected to an online gas chromatograph (Shimadzu GC-8A) equipped with a thermal conductivity detector. The chemical compositions of all the samples were analyzed by using a PANalytical Axios X-ray fluorescence spectrometer. X-ray photoelectron spectra were recorded by using a VG ESCALAB MK-II spectrometer with a sample transfer system. TOF-SIMS investigations were performed by using an IONTOF instrument equipped with a Bi⁺ primary ion source in the static mode. Temperature-programmed oxidation (TPO) experiments were performed in a U-shaped quartz microreactor with an online Omnistar mass spectrometer. (Detailed descriptions are provided in the Supporting Information.)

Catalyst evaluation

The catalytic test was performed in a fixed-bed flow microreactor with an inner diameter of 7 mm. The reaction temperature was measured with a coaxial thermocouple, the end of which was fixed in the middle of the catalyst bed. In each experiment, the catalyst (0.5 g) was charged at the center of the reactor. Conventionally, the catalyst was pretreated in situ at 550 °C with inert N_2 (20 mL min⁻¹) for 2 h, and then the system was cooled down to the desired reaction temperature under N_2 flow. Afterwards, 1-butene feed with a weight hourly space velocity of 1.5 h⁻¹ was introduced into the reactor. The reaction products were analyzed by an online Varian CP 3800 gas chromatograph equipped with a flame ionization detector. The connecting lines between the reactor outlet and the sampling valve were heated to prevent conden-

sation of the products with high molecular weights. Quantitative analyses of the products were calculated by using the corrected area normalization method, and carbonaceous deposits on catalysts were not taken into account for the calculation.

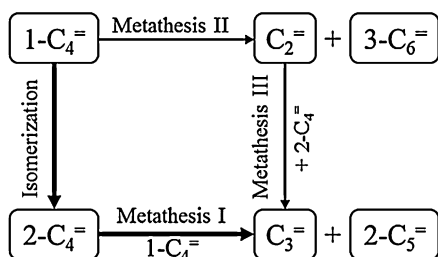
Isomers of 1-butene, that is, *cis*-2-butene and *trans*-2-butene produced from the isomerization of 1-butene, were considered to be unconverted feedstock. The conversion (*X*) of 1-butene and the yield (*Y*) to a particular product were calculated by using Equations (1) and (2):

$$X(1-C_4^=) = \frac{[1-C_4^=]_F - [1-C_4^=]_P - [2-C_4^=]_P}{[1-C_4^=]_F} \times 100\% \quad (1)$$

$$Y(C_n^=) = \frac{X(1-C_4^=) \times [C_n^=]_P}{[C_2^=]_P + [C_3^=]_P + [C_5^=]_P + [C_6^=]_P + [C_7^+]_P} \times 100\% \quad (2)$$

in which $[1-C_4^=]_F$ represents the weight percent of 1-butene in the feed; $[C_2^=]_P$, $[C_3^=]_P$, $[2-C_4^=]_P$, $[C_5^=]_P$, $[C_6^=]_P$, and $[C_7^+]_P$ are the weight percentages of each component in the products, respectively; $Y(C_n^=)$ is the product yield with the carbon number *n*. In addition, C_7^+ denotes all the heavy products having seven or more carbon atoms.

Scheme 1 illustrates the main possible reaction pathways for the metathesis of 1-butene over Mo-based catalysts.^[14,61] Desired propene could come from metathesis of 2-butene and 1-butene (metathesis I) and metathesis of ethene and 2-butene (metathesis III). 1-Butene isomerization to 2-butene as the prerequisite step of metathesis I and self-metathesis of 1-butene to ethene and hexene (metathesis II) is an alternative route for the production of propene through metathesis III.^[14]



Scheme 1. Reaction pathways for the autometathesis of 1-butene over Mo-based catalysts, as proposed in Ref. [64].

Acknowledgements

We are grateful for financial support from the National Natural Science Foundation of China (Grant Nos. 20903088 and 21376235).

Keywords: alumina · metathesis · molybdenum · propene · sba-15

[1] E. Mazoyer, K. C. Szeto, N. Merle, S. Norsic, O. Boyron, J.-M. Basset, M. Taoufik, C. P. Nicholas, *J. Catal.* **2013**, *301*, 1–7.

- [2] C. Angelici, B. M. Weckhuysen, P. C. A. Bruijninx, *ChemSusChem* **2013**, *6*, 1595–1614.
- [3] M. Stöcker, *Microporous Mesoporous Mater.* **1999**, *29*, 3–48.
- [4] F. Cavani, N. Ballarini, A. Cericola, *Catal. Today* **2007**, *127*, 113–131.
- [5] X. X. Zhu, S. L. Liu, Y. Q. Song, S. J. Xie, L. Y. Xu, *Appl. Catal. A* **2005**, *290*, 191–199.
- [6] C. Lin, K. Tao, H. B. Yu, D. Y. Hua, S. H. Zhou, *Catal. Sci. Technol.* **2014**, *4*, 4010–4019.
- [7] D. P. Debecker, K. Bouchmella, M. Stoyanova, U. Rodemerck, E. M. Gaigneaux, P. H. Mutin, *Catal. Sci. Technol.* **2012**, *2*, 1157–1164.
- [8] R. L. Banks, G. C. Bailey, *I&EC Prod. Res. Dev.* **1964**, *3*, 170–173.
- [9] J. C. Mol, *J. Mol. Catal. A* **2004**, *213*, 39–45.
- [10] J. Engelhardt, D. Kallo, I. Zsinka, *J. Catal.* **1984**, *88*, 317–324.
- [11] Y. D. Wang, Q. L. Chen, W. M. Yang, Z. K. Xie, X. Xu, D. Huang, *Appl. Catal. A* **2003**, *250*, 25–37.
- [12] D. P. Debecker, M. Stoyanova, F. Colbeau-Justin, U. Rodemerck, C. Bois-siere, E. M. Gaigneaux, C. Sanchez, *Angew. Chem. Int. Ed.* **2012**, *51*, 2129–2131; *Angew. Chem.* **2012**, *124*, 2171–2173.
- [13] E. Mazoyer, K. C. Szeto, S. Norsic, A. Garron, J. M. Basset, C. P. Nicholas, M. Taoufik, *ACS Catal.* **2011**, *1*, 1643–1646.
- [14] X. J. Li, D. Z. Zhang, X. X. Zhu, F. C. Chen, S. L. Liu, S. J. Xie, L. Y. Xu, *J. Mol. Catal. A* **2013**, *372*, 121–127.
- [15] L. Harmse, C. van Schalkwyk, E. van Steen, *Catal. Lett.* **2010**, *137*, 123–131.
- [16] D. Y. Zhao, Q. S. Huo, J. L. Feng, B. F. Chmelka, G. D. Stucky, *J. Am. Chem. Soc.* **1998**, *120*, 6024–6036.
- [17] X. Li, W. Zheng, H. Pan, Y. Yu, L. Chen, P. Wu, *J. Catal.* **2013**, *300*, 9–19.
- [18] O. Y. Gutierrez, D. Valencia, G. A. Fuentes, T. Klimova, *J. Catal.* **2007**, *249*, 140–153.
- [19] J. C. Hu, Y. D. Wang, L. F. Chen, R. Richards, W. M. Yang, Z. C. Liu, W. Xu, *Microporous Mesoporous Mater.* **2006**, *93*, 158–163.
- [20] T. I. Bhuiyan, P. Arudra, M. N. Akhtar, A. M. Aitani, R. H. Abudawoud, M. A. Al-Yami, S. S. Al-Khattaf, *Appl. Catal. A* **2013**, *467*, 224–234.
- [21] B. Hu, H. Liu, K. Tao, C. R. Xiong, S. H. Zhou, *J. Phys. Chem. C* **2013**, *117*, 26385–26395.
- [22] P. Topka, H. Balcar, J. Rathousky, N. Zilkova, F. Verpoort, J. Cejka, *Microporous Mesoporous Mater.* **2006**, *96*, 44–54.
- [23] H. Balcar, D. Mishra, E. Marceau, X. Carrier, N. Zilkova, Z. Bastl, *Appl. Catal. A* **2009**, *359*, 129–135.
- [24] H. Balcar, J. Cejka, *Coord. Chem. Rev.* **2013**, *257*, 3107–3124.
- [25] D. P. Debecker, K. Bouchmella, C. Poleunis, P. Eloy, P. Bertrand, E. M. Gaigneaux, P. H. Mutin, *Chem. Mater.* **2009**, *21*, 2817–2824.
- [26] D. P. Debecker, B. Schimmoeller, M. Stoyanova, C. Poleunis, P. Bertrand, U. Rodemerck, E. M. Gaigneaux, *J. Catal.* **2011**, *277*, 154–163.
- [27] K. Bouchmella, P. H. Mutin, M. Stoyanova, C. Poleunis, P. Eloy, U. Rodemerck, E. M. Gaigneaux, D. P. Debecker, *J. Catal.* **2013**, *301*, 233–241.
- [28] N. Liu, S. L. Ding, Y. M. Cui, N. H. Xue, L. M. Peng, X. F. Guo, W. P. Ding, *Chem. Eng. Res. Des.* **2013**, *91*, 573–580.
- [29] D. Y. Zhao, J. L. Feng, Q. S. Huo, N. Melosh, G. H. Fredrickson, B. F. Chmelka, G. D. Stucky, *Science* **1998**, *279*, 548–552.
- [30] K. K. Cheralathan, T. Hayashi, M. Ogura, *Microporous Mesoporous Mater.* **2008**, *116*, 406–415.
- [31] A. García-Trenco, A. Martínez, *Catal. Today* **2013**, *215*, 152–161.
- [32] M. Shakeri, R. Gebbink, P. E. de Jongh, K. P. de Jong, *Microporous Mesoporous Mater.* **2013**, *170*, 340–345.
- [33] X. Y. Liu, L. B. Sun, F. Lu, T. T. Li, X. Q. Liu, *J. Mater. Chem. A* **2013**, *1*, 1623–1631.
- [34] X. Y. She, J. H. Kwak, J. M. Sun, J. Z. Hu, M. Y. Hu, C. M. Wang, C. H. F. Peden, Y. Wang, *ACS Catal.* **2012**, *2*, 1020–1026.
- [35] P. C. Bakala, E. Briot, Y. Millot, J. Y. Piquemal, J. M. Bregault, *J. Catal.* **2008**, *258*, 61–70.
- [36] C. Pecharrmán, I. Sobrados, J. E. Iglesias, T. Gonzalez-Carreno, J. Sanz, *J. Phys. Chem. B* **1999**, *103*, 6160–6170.
- [37] B. M. De Witte, P. J. Grobet, J. B. Uytterhoeven, *J. Phys. Chem.* **1995**, *99*, 6961–6965.
- [38] A. H. Tavakoli, P. S. Maram, S. J. Widgeon, J. Rufner, K. van Benthem, S. Ushakov, S. Sen, A. Navrotsky, *J. Phys. Chem. C* **2013**, *117*, 17123–17130.
- [39] A. Goldbourt, M. V. Landau, S. Vega, *J. Phys. Chem. B* **2003**, *107*, 724–731.
- [40] H. N. Wang, X. H. Li, Y. M. Wang, P. Wu, *ChemCatChem* **2010**, *2*, 1303–1311.

- [41] R. Vidruk, M. V. Landau, M. Herskowitz, V. Ezersky, A. Goldbourt, *J. Catal.* **2011**, *282*, 215–227.
- [42] J. M. R. Gallo, C. Bisio, G. Gatti, L. Marchese, H. O. Pastore, *Langmuir* **2010**, *26*, 5791–5800.
- [43] T. Klimova, J. Reyes, O. Gutierrez, L. Lizama, *Appl. Catal. A* **2008**, *335*, 159–171.
- [44] X. S. Liu, R. E. Truitt, *J. Am. Chem. Soc.* **1997**, *119*, 9856–9860.
- [45] Y. C. Lou, H. C. Wang, Q. H. Zhang, Y. Wang, *J. Catal.* **2007**, *247*, 245–255.
- [46] K. Amakawa, L. L. Sun, C. S. Guo, M. Havecker, P. Kube, I. E. Wachs, S. Lwin, A. I. Frenkel, A. Patlolla, K. Hermann, R. Schlogl, A. Trunschke, *Angew. Chem. Int. Ed.* **2013**, *52*, 13553–13557; *Angew. Chem.* **2013**, *125*, 13796–13800.
- [47] X. J. Li, W. P. Zhang, S. L. Liu, L. Y. Xu, X. W. Han, X. H. Bao, *J. Catal.* **2007**, *250*, 55–66.
- [48] F. De Smet, M. Devillers, C. Poleunis, P. Bertrand, *J. Chem. Soc. Faraday Trans.* **1998**, *94*, 941–947.
- [49] L.-T. Weng, *Appl. Catal. A* **2014**, *474*, 203–210.
- [50] S. Rondon, W. R. Wilkinson, A. Proctor, M. Houalla, D. M. Hercules, *J. Phys. Chem.* **1995**, *99*, 16709–16713.
- [51] M. Sibeijn, R. Spronk, J. A. R. Vanveen, J. C. Mol, *Catal. Lett.* **1991**, *8*, 201–208.
- [52] T. Kitano, S. Okazaki, T. Shishido, K. Teramura, T. Tanaka, *J. Mol. Catal. A* **2013**, *371*, 21–28.
- [53] S. L. Liu, S. J. Huang, W. J. Xin, J. Bai, S. J. Xie, L. Y. Xu, *Chem. Res. Chin. Univ.* **2005**, *21*, 213–216.
- [54] L. Alvarado Perea, T. Wolff, P. Veit, L. Hilfert, F. T. Edelmann, C. Hamel, A. Seidel-Morgenstern, *J. Catal.* **2013**, *305*, 154–168.
- [55] H. J. Liu, S. J. Huang, L. Zhang, S. L. Liu, W. Wang, W. J. Xin, S. J. Xie, L. Y. Xu, *Chin. J. Catal.* **2008**, *29*, 513–518.
- [56] W. H. Meyer, M. M. D. Radebe, D. W. Serfontein, U. Ramdhani, M. du Toit, C. P. Nicolaides, *Appl. Catal. A* **2008**, *340*, 236–241.
- [57] K. Amakawa, S. Wrabetz, J. Krohnert, G. Tzolova-Muller, R. Schlögl, A. Trunschke, *J. Am. Chem. Soc.* **2012**, *134*, 11462–11473.
- [58] X. J. Li, W. P. Zhang, X. Li, S. L. Liu, H. J. Huang, X. W. Han, L. Y. Xu, X. H. Bao, *J. Phys. Chem. C* **2009**, *113*, 8228–8233.
- [59] H. Aritani, O. Fukuda, T. Yamamoto, T. Tanaka, S. Imamura, *Chem. Lett.* **2000**, 66–67.
- [60] J. Handzlik, P. Sautet, *J. Catal.* **2008**, *256*, 1–14.
- [61] S. J. Huang, H. J. Liu, L. Zhang, S. L. Liu, W. J. Xin, X. J. Li, S. J. Xie, L. Y. Xu, *Appl. Catal. A* **2011**, *404*, 113–119.
- [62] C. K. Krishnan, T. Hayashi, M. Ogura, *Adv. Mater.* **2008**, *20*, 2131–2136.
- [63] P. Iengo, M. Di Serio, A. Sorrentino, V. Solinas, E. Santacesaria, *Appl. Catal. A* **1998**, *167*, 85–101.
- [64] X. J. Li, X. X. Zhu, D. Z. Zhang, F. C. Chen, P. Zeng, S. L. Liu, S. J. Xie, L. Y. Xu, *J. Energy Chem.* **2013**, *22*, 145–150.

Manuscript received: April 5, 2015

Accepted article published: May 22, 2015

Final article published: June 25, 2015